

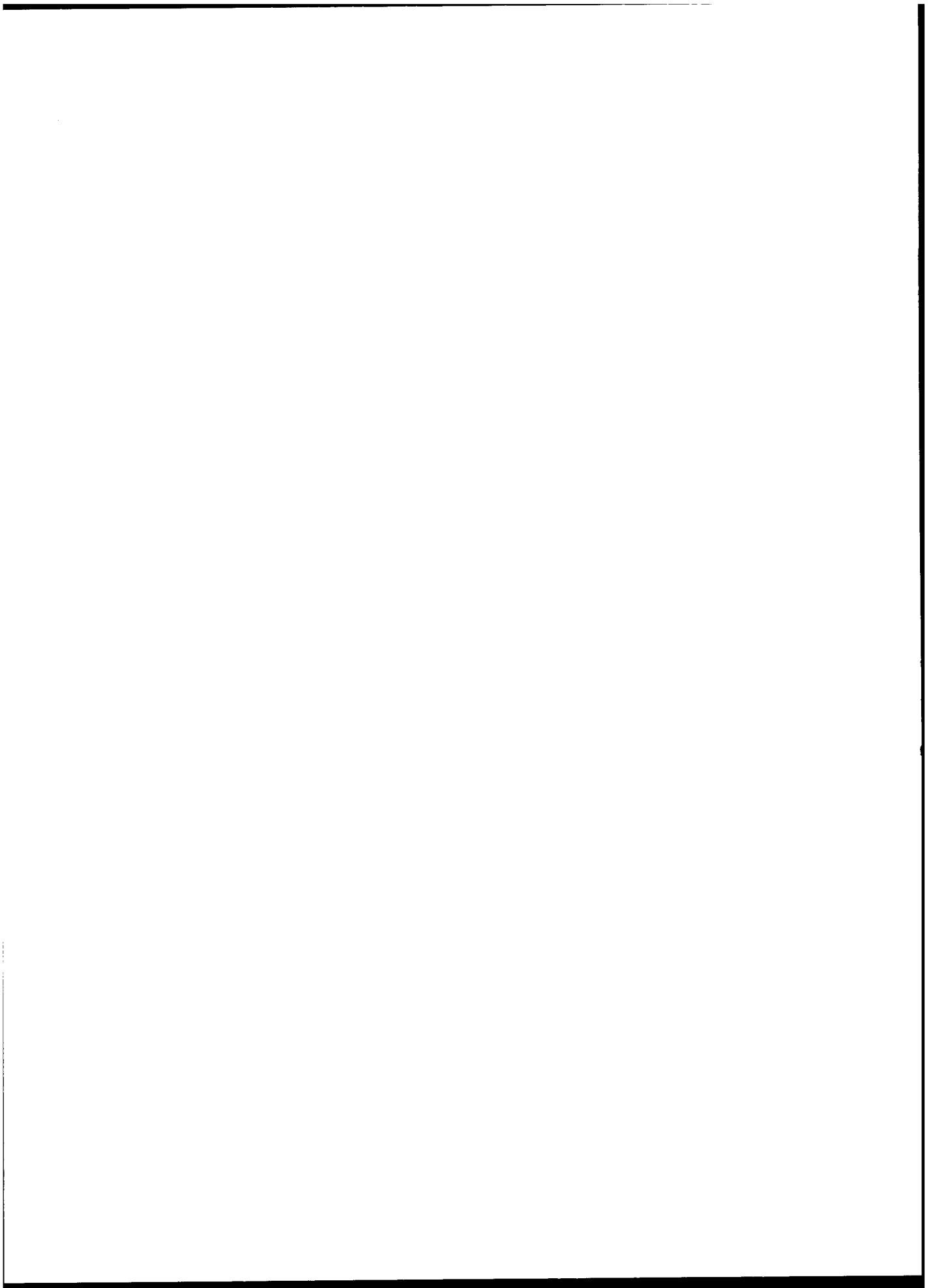
REPORT DOCUMENTATION PAGE		READ INSTRUCTIONS BEFORE COMPLETING FORM
1. REPORT NUMBER NRL Report 7820	2. GOVT ACCESSION NO.	3. RECIPIENT'S CATALOG NUMBER
4. TITLE (and Subtitle) MICROSTRUCTURE AND SWELLING OF FAST NEUTRON IRRADIATED TYPE 304 STAINLESS STEEL		5. TYPE OF REPORT & PERIOD COVERED Interim
		6. PERFORMING ORG. REPORT NUMBER
7. AUTHOR(s) D.J. Michel, H.H. Smith, and J.T. Atwell		8. CONTRACT OR GRANT NUMBER(s)
9. PERFORMING ORGANIZATION NAME AND ADDRESS Naval Research Laboratory Washington, D.C. 20375		10. PROGRAM ELEMENT, PROJECT, TASK AREA & WORK UNIT NUMBERS NRL Problem MO1-27 and MO1-14, RR022-11-41-5426, RR022-11-41-5409
11. CONTROLLING OFFICE NAME AND ADDRESS Department of the Navy Office of Naval Research Arlington, Va. 22217		12. REPORT DATE December 9, 1974
		13. NUMBER OF PAGES 21
14. MONITORING AGENCY NAME & ADDRESS (if different from Controlling Office)		15. SECURITY CLASS. (of this report) Unclassified
		15a. DECLASSIFICATION/DOWNGRADING SCHEDULE
16. DISTRIBUTION STATEMENT (of this Report) Approved for public release; distribution unlimited.		
17. DISTRIBUTION STATEMENT (of the abstract entered in Block 20, if different from Report)		
18. SUPPLEMENTARY NOTES Also sponsored by the U.S. Atomic Energy Commission		
19. KEY WORDS (Continue on reverse side if necessary and identify by block number)		
Dislocations	Radiation effects	
Immersion density	Stainless steel	
Microhardness	Swelling	
Microstructure	Transmission electron microscopy	
Neutron Irradiation	Voids	
20. ABSTRACT (Continue on reverse side if necessary and identify by block number)		
<p>The effects of high-fluence, fast-neutron irradiation on the microstructure, swelling, and microhardness were evaluated for annealed Type 304 stainless steel that had attained fluences near 1.6×10 to the 23rd power n/sq cm > 0.1 MeV at irradiation temperatures from 370C to 470C (698F to 878F). Transmission electron microscopy was employed to characterize the radiation-induced void and defect structures. A maximum swelling of 10.4% was determined by immersion density measurements and independently confirmed from the microscopy data. Ambient temperature microhardness measurements were found to be in general agreement with calculated</p> <p style="text-align: right;">(Continued)</p>		

20. Abstract

microhardness values based on the microscopy data. The calculations indicate that the radiation-induced voids were the primary microstructural component responsible for the measured microhardness. All results show the strong influence of the irradiation temperature and neutron-fluence gradients experienced by the material during the EBR-II exposure.

CONTENTS

INTRODUCTION	1
EXPERIMENTAL PROCEDURES	1
RESULTS AND DISCUSSION	3
SUMMARY AND CONCLUSIONS	15
ACKNOWLEDGMENTS	16
REFERENCES	16



MICROSTRUCTURE AND SWELLING OF FAST NEUTRON IRRADIATED TYPE 304 STAINLESS STEEL

INTRODUCTION

The austenitic stainless steels have been selected for use as the structural components and fuel cladding in the future liquid metal fast breeder reactors (LMFBR). This application has necessitated the development of considerable data concerning the effects of elevated-temperature fast-neutron irradiation on the microstructure and properties of these steels. Extensive postirradiation studies have been conducted to examine the effects of high-fluence irradiation on the swelling behavior and microstructure of both Type 304 and Type 316 steel [1-12]. Other studies have examined the postirradiation tensile [13-16], creep [17-20], and fatigue [21-27] properties of these steels.

An important source of material for many studies has been the structural components of the Experimental Breeder Reactor No. II (EBR-II). These annealed Type 304 stainless steel components are of considerable interest because they have attained the highest fast neutron fluences of currently available material. Consequently, the swelling behavior, microstructure, and tensile properties of these components have been evaluated in detail [1-7, 14]. These studies include a recently reported NRL evaluation of the fatigue behavior of thin section Type 304 stainless steel control rod thimble material [27].

In the present study, the microstructure and swelling of the annealed Type 304 stainless steel thimble material were examined by transmission electron microscopy (TEM) and immersion density methods. Microhardness measurements were performed to determine the flow properties of the material and for correlation with the microstructure data. The results illustrate the strong effects of irradiation temperature and neutron fluence on the microstructure and properties of the thimble material.

EXPERIMENTAL PROCEDURES

The annealed Type 304 stainless steel used in this study was taken from flat 4 of the upper section of EBR-II control rod guide thimble 5D3. This material was removed from the reactor after accumulating 42,321 MW-days of reactor exposure and a maximum calculated neutron fluence of 1.6×10^{23} n/cm² > 0.1 MeV. The axial irradiation temperature and fluence distributions for the material are shown in Fig. 1.

The TEM, immersion density, and microhardness specimens were prepared from the unstrained end sections of the previously prepared and tested fatigue specimens [27]. Both the TEM and microhardness specimens were approximately 3.2 mm square by 1 mm thick. For TEM examination, the specimens were first reduced in thickness to 0.25 mm by careful, low-speed grinding. A twin jet electropolishing method [28] was found to produce excellent thin foils for the subsequent TEM examinations conducted at 200 kV with a JEM 200A transmission electron microscope.

Note: Manuscript submitted September 4, 1974.

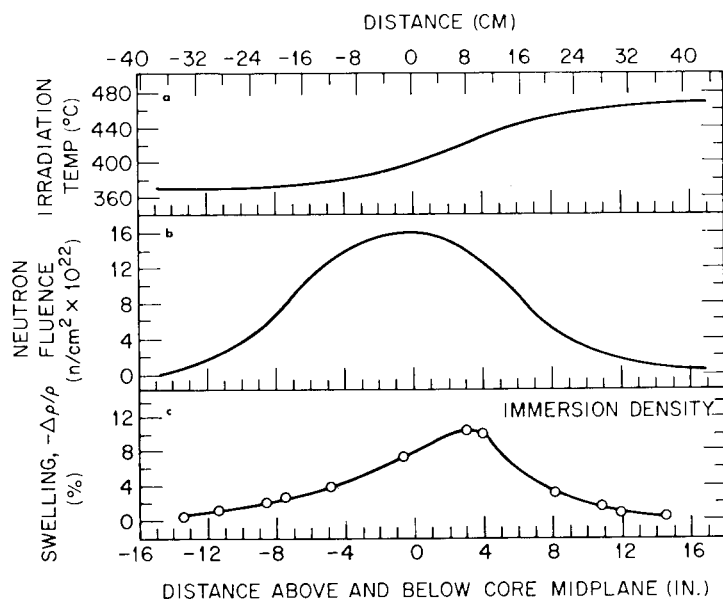


Fig. 1 — Irradiation temperature (a), neutron fluence (b), and swelling (immersion density change) (c) profiles for neutron-irradiated Type 304 stainless steel (EBR-II control rod thimble 5D3, flat number 4)

The radiation-induced voids present in all specimens were observed and photographed in the underfocused condition. A Zeiss particle-size analyzer was used to determine the void size. The stereographic method was employed to obtain the foil thicknesses for calculation of the void number density per unit volume. The void number densities are estimated to be accurate within $\pm 25\%$.

The specimens employed for the immersion density measurements were approximately 3.2 mm wide by 25 mm long by 1 mm thick. The mass of all specimens was approximately 0.5 g. The specimens received no special surface preparation except that all rough edges remaining from the cutting operations were removed by lightly abrading the specimen edges. The method used to determine the density changes was similar to that employed by Ratcliffe [29]. According to this method, the change in density $\Delta \rho / \rho$ of a specimen having weight W_a in air and weight W_l in liquid, when compared to a standard or dummy specimen having weight w_a in air and weight w_l in liquid, may be expressed as

$$\frac{\Delta \rho}{\rho} = 1 - \frac{w_a - w_l}{W_a - W_l} \frac{W_a}{W_l} \quad (1)$$

Distilled water containing a minor concentration of a surface wetting agent (Photo-Flo) was used as the immersion liquid. A semimicro analytical balance capable of being read to the nearest $10 \mu\text{g}$ was employed for the measurements. The immersion density measurements are estimated to be accurate to $\pm 0.1\%$.

Specimens suitable for microhardness measurements were prepared by mounting the 3.2mm square specimen blanks in polyester resin and lightly abrading the exposed surface to remove any mounting material or surface oxide. The specimens were electro-polished with a 5HCl:10₄:15H₂O:80CH₃OOH (by volume) electrolyte to produce smooth and stain-free surfaces. The microhardness measurements were made with a 136-degree diamond pyramid indenter at room temperature using a 1-kg load. At least three indents were used to obtain the reported hardness values.

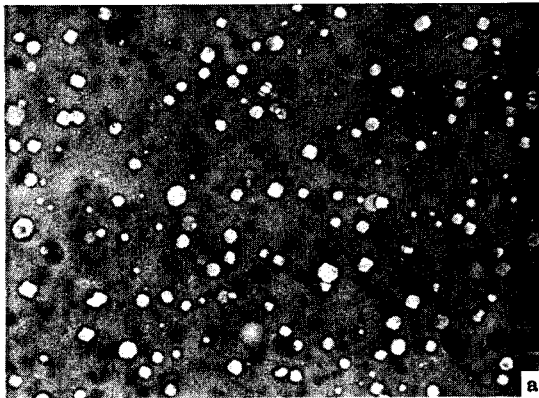
RESULTS AND DISCUSSION

Radiation-induced voids were observed in the thimble material at all irradiation temperatures and neutron fluences. Figure 2 illustrates the inhomogeneous void distributions for those TEM specimens previously exposed to the 427°C (800°F) fatigue test temperature. With increasing irradiation temperature, it is clearly evident that the void size generally increased and the void number density decreased. Similar trends also are seen in Fig. 3 for those TEM specimens previously exposed to the 593°C (1100°F) fatigue test temperature. For all specimens, however, the effect of the neutron fluence gradient produced a maximum in the mean void diameter near the maximum fluence location.

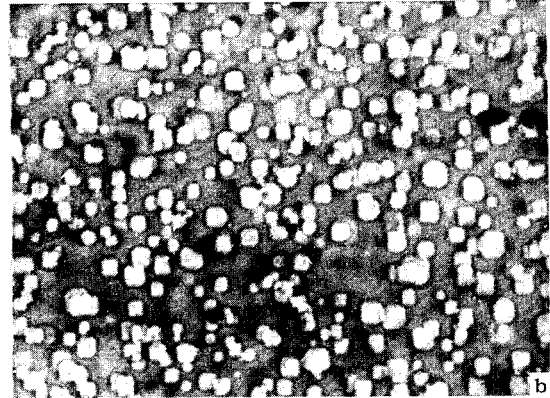
The influence of grain boundaries on the void formation is shown in Fig. 4. In Figs. 4a and 4d, zones adjacent to the grain boundary approximately 1000 to 2000 Å wide are denuded of void formation. Similar denuding was observed throughout those specimens irradiated to low fluences at both the lower and higher irradiation temperatures. Specimens irradiated to the higher fluences at the intermediate irradiation temperatures, however, exhibited no void denuding at the grain boundaries. Typical examples are seen in Figs. 4b and 4c in which the matrix void distribution extends to the grain boundaries. Also evident in Fig. 4 are the grain boundary precipitates, predominantly of the M₂₃C₆ type, which were observed in all specimens and whose size increased with increasing irradiation temperature.

An interesting feature of all TEM specimens was the observation of matrix areas where clusters of many small voids were present. Two examples are seen in Figs. 5a and 5b. Other matrix areas exhibited small holes as seen in Figs. 5c and 5d. Because both large and small matrix precipitates also were observed in all specimens, it is suspected that removal of the large precipitates during the foil preparation was responsible for the holes and that the small voids directly reflect the solute segregation in the vicinity of the large precipitates. It is possible in several specimens, however, that the coalescence of several smaller voids within the matrix occurred to produce a larger void that exceeded the foil thickness after thinning. The small M₂₃C₆ precipitates within the matrix were observed to be randomly distributed and generally not associated with the voids.

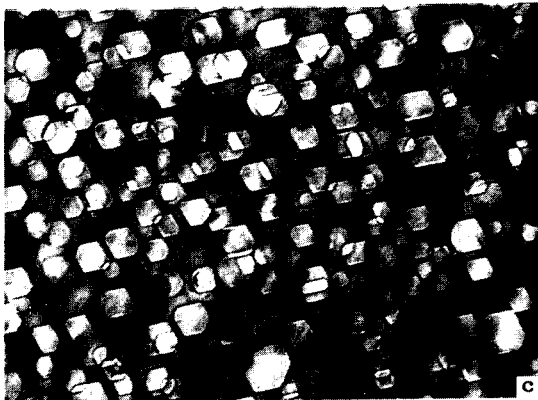
The transmission electron microscopy, immersion density, and microhardness results are summarized in Table 1. From an examination of the table, it is evident that the effects of both irradiation temperature and neutron fluence strongly influenced the mean void diameters, void number densities, and the resultant specimen volume change.



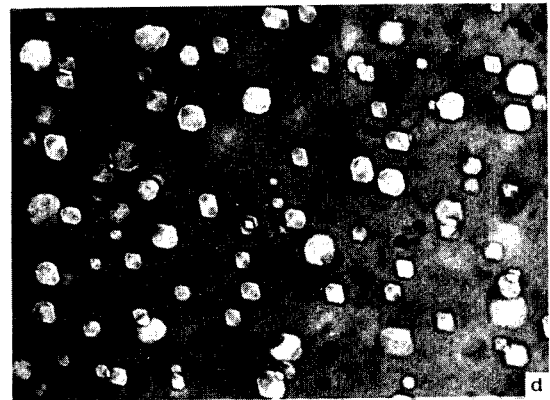
$T_{\text{irrad}} = 371^{\circ}\text{C}$, $\phi t = 6.0 \times 10^{22} \text{ n/cm}^2$



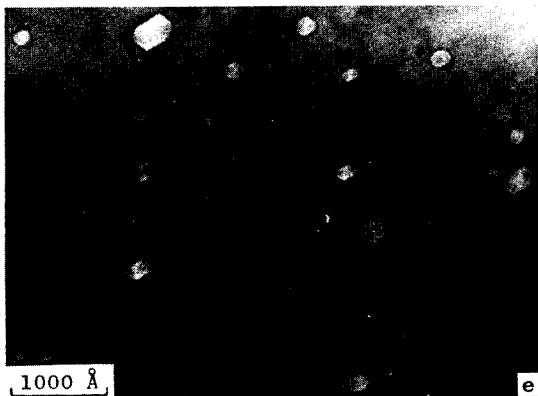
$T_{\text{irrad}} = 388^{\circ}\text{C}$, $\phi t = 1.3 \times 10^{23} \text{ n/cm}^2$



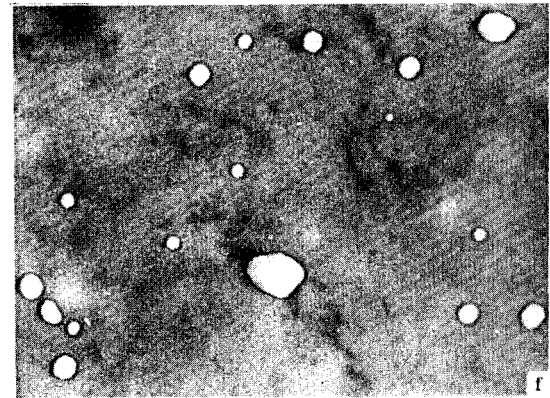
$T_{\text{irrad}} = 415^{\circ}\text{C}$, $\phi t = 1.6 \times 10^{23} \text{ n/cm}^2$



$T_{\text{irrad}} = 449^{\circ}\text{C}$, $\phi t = 7.0 \times 10^{22} \text{ n/cm}^2$

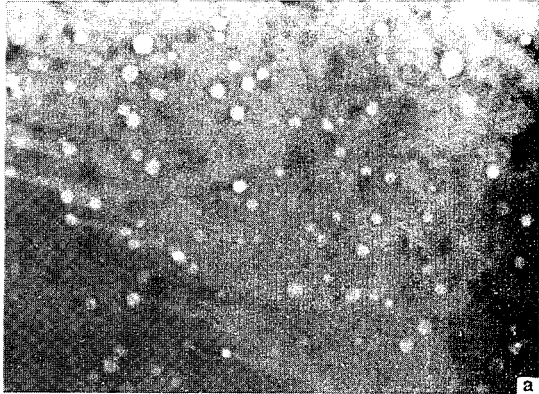


$T_{\text{irrad}} = 460^{\circ}\text{C}$, $\phi t = 1.4 \times 10^{22} \text{ n/cm}^2$

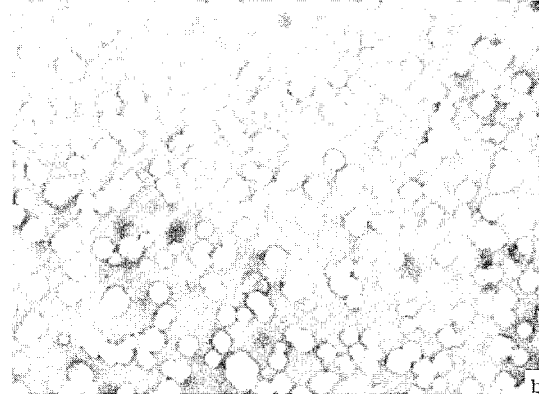


$T_{\text{irrad}} = 471^{\circ}\text{C}$, $\phi t = 9.0 \times 10^{21} \text{ n/cm}^2$

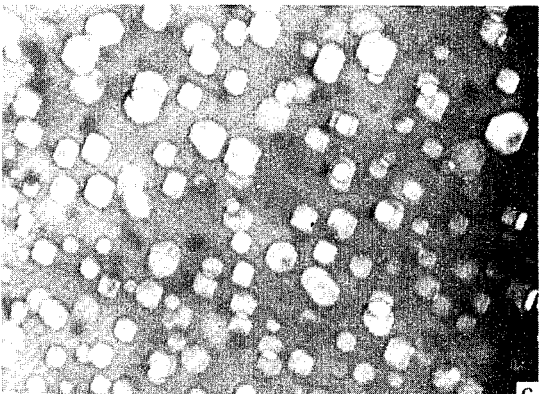
Fig. 2 — Transmission electron micrographs of radiation-induced voids in neutron-irradiated Type 304 stainless steel (EBR-II control rod thimble 5D3). Specimen material, except (c), received post-irradiation thermal exposure at 427°C (800°F) during fatigue tests.



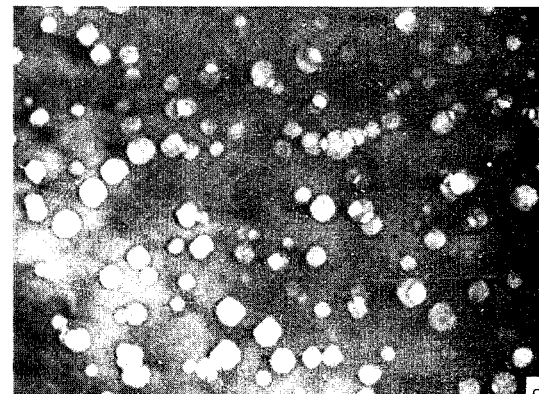
$T_{\text{irrad}} = 371^{\circ}\text{C}$, $\phi t = 1.3 \times 10^{22} \text{ n/cm}^2$



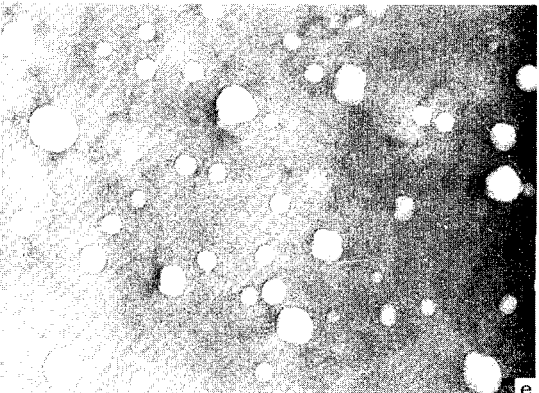
$T_{\text{irrad}} = 382^{\circ}\text{C}$, $\phi t = 1.3 \times 10^{22} \text{ n/cm}^2$



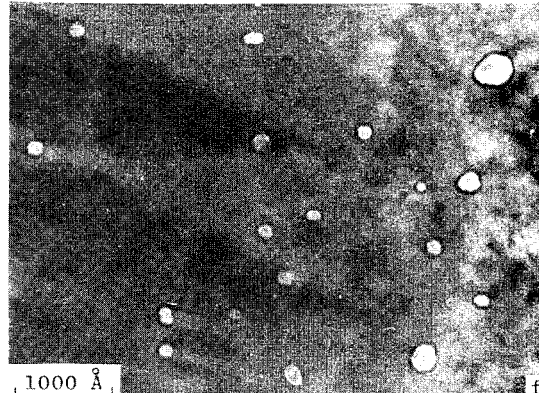
$T_{\text{irrad}} = 438^{\circ}\text{C}$, $\phi t = 1.0 \times 10^{22} \text{ n/cm}^2$



$T_{\text{irrad}} = 449^{\circ}\text{C}$, $\phi t = 7.0 \times 10^{22} \text{ n/cm}^2$



$T_{\text{irrad}} = 460^{\circ}\text{C}$, $\phi t = 1.4 \times 10^{22} \text{ n/cm}^2$



$T_{\text{irrad}} = 471^{\circ}\text{C}$, $\phi t = 9.0 \times 10^{21} \text{ n/cm}^2$

Fig. 3 — Transmission electron micrographs of radiation-induced voids in neutron irradiated Type 304 stainless steel (EBR-II control rod thimble 5D3). Specimen material received postirradiation thermal exposure at 593°C (1100°F) during fatigue tests.

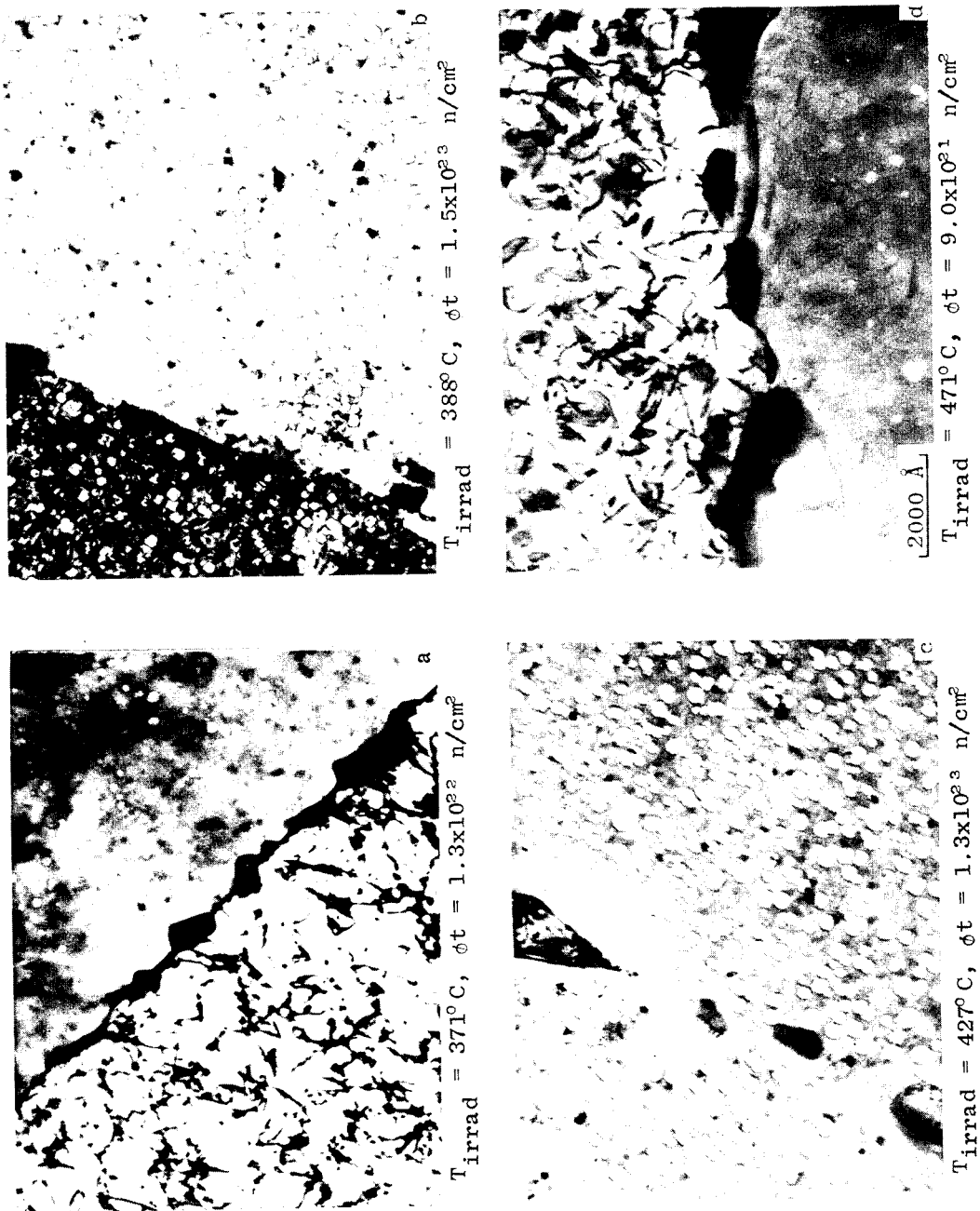
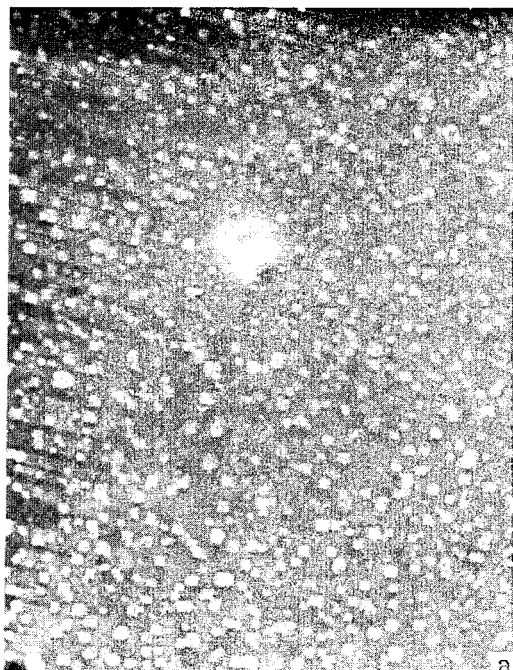


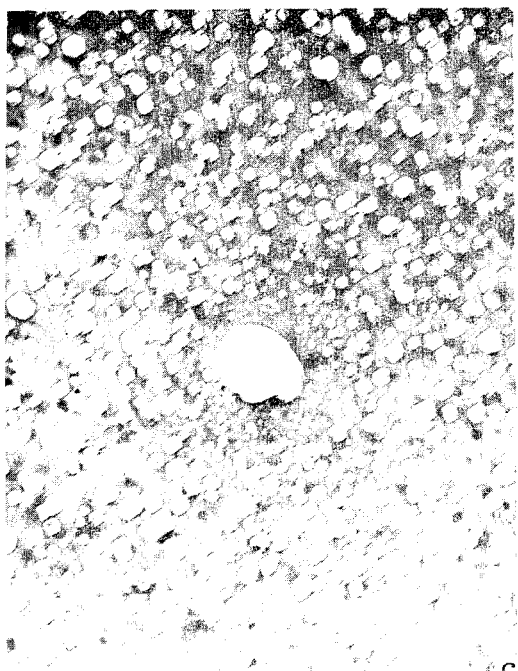
Fig. 4 — Transmission electron micrographs of grain boundary areas in neutron-irradiated Type 304 stainless steel (EBR-II control rod thimble 5D3). Note void denuding at grain boundaries in (a) and (d) and precipitate formation at boundaries in (a) through (d).



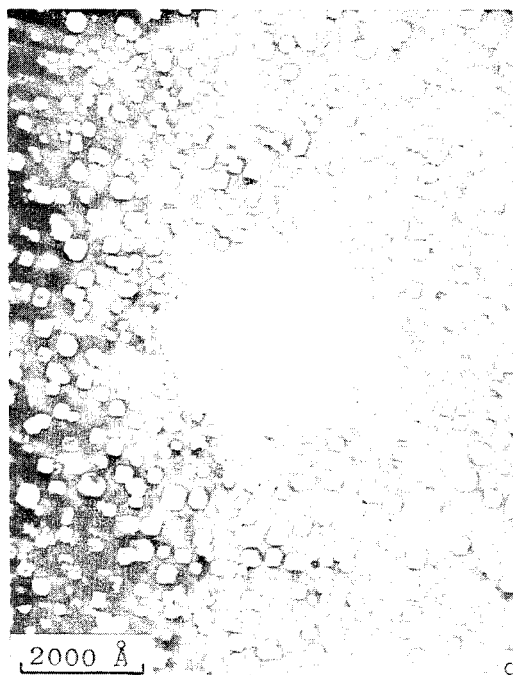
$T_{\text{irrad}} = 388^{\circ}\text{C}$, $\phi t = 1.5 \times 10^{23} \text{ n/cm}^2$



$T_{\text{irrad}} = 427^{\circ}\text{C}$, $\phi t = 1.3 \times 10^{23} \text{ n/cm}^2$



$T_{\text{irrad}} = 415^{\circ}\text{C}$, $\phi t = 1.6 \times 10^{23} \text{ n/cm}^2$



$T_{\text{irrad}} = 438^{\circ}\text{C}$, $\phi t = 1.0 \times 10^{23} \text{ n/cm}^2$

Fig. 5 — Transmission electron micrographs of matrix regions in neutron-irradiated Type 304 stainless steel (EBR-II control rod thimble 5D3) showing the appearance of radiation-induced voids near the suspected location of large precipitates. The precipitates were removed during the microscope specimen preparation.

Table 1
 Summary of Microstructure Data for Solution Treated Type 304 Stainless Steel
 EBR-II Control Rod Thimble 5D3

Specimen Number	Distance Above or Below Core Midplane* (in.)	Neutron Fluence† (total n/cm ²)	Irradiation Temperature‡ (°C)	Test Temp‡ (°C)	Microhardness ΔH (kg/mm ²)	TEM DATA				Swelling § (Immersion Density Change) -Δρ/ρ(%)	
						Dislocation Density (#/cm ³)	Mean Void Diameter (Å)	No. of Voids Measured	Void Number Density (#/cm ³)		Void Volume (Calculated) ΔV/V(%)
1	-12.25	1.3X10 ²²	371	427	179	-	102	519	1.1X10 ¹⁶	0.83	1.56
2	-9.60	6.0X10 ²²	371	593	135	4.0X10 ¹⁰	131	328	1.3X10 ¹⁶	1.75	2.03
3	-6.50	1.0X10 ²³	371	427	215	-	-	-	-	-	2.84
4	-3.80	1.3X10 ²³	382	593	137	1.3X10 ¹⁰	162	413	8.2X10 ¹⁵	2.23	3.99
5	-1.60	1.5X10 ²³	388	427	192	1.9X10 ¹⁰	180	1153	8.0X10 ¹⁵	3.06	7.54
7	7.20	1.0X10 ²³	438	-	100	1.1X10 ¹⁰	228	590	2.5X10 ¹⁵	1.94	2.69
8	9.90	7.0X10 ²²	449	593	90	1.1X10 ¹⁰	188	392	4.1X10 ¹⁵	1.95	1.73
9	13.00	1.4X10 ²²	460	427	91	9.0X10 ⁹	180	502	7.4X10 ¹⁴	0.35	1.08
10	15.70	9.0X10 ²¹	471	593	80	1.5X10 ¹⁰	179	676	2.8X10 ¹⁴	0.21	0.97
15	-12.25	1.3X10 ²²	371	593	100	9.6X10 ⁹	134	250	1.6X10 ¹⁵	0.25	1.29
16	-9.60	6.0X10 ²²	371	427	187	4.1X10 ¹⁰	116	636	5.8X10 ¹⁵	0.68	2.11
22	5.00	1.3X10 ²³	427	427	86	3.4X10 ¹⁰	260	243	8.7X10 ¹⁵	9.96	10.25
23	7.20	1.0X10 ²³	438	593	99	1.7X10 ¹⁰	232	432	5.3X10 ¹⁵	4.37	3.79
24	9.90	7.0X10 ²²	449	427	121	1.9X10 ¹⁰	201	566	3.6X10 ¹⁵	2.10	2.18
25	13.00	1.4X10 ²²	460	593	90	1.7X10 ¹⁰	210	715	9.2X10 ¹⁴	0.65	1.63
26	15.70	9.0X10 ²¹	471	427	94	1.0X10 ¹⁰	186	658	4.4X10 ¹⁴	0.23	0.74
34	3.00	1.4X10 ²³	415	-	144	-	264	602	8.8X10 ¹⁵	10.40	10.40
35	-13.50	9.0X10 ²¹	371	-	195	-	98†	453	1.2X10 ¹⁶	0.93	1.19

Location of fatigue specimens. Specimens for immersion density and TEM displaced slightly in location.

† Calculated from EBR-II supplied data.

‡ Temperature at which fatigue tests were conducted.

Increase in ambient temperature microhardness when compared with unirradiated thimble stock.

§ Density of unirradiated thimble stock determined to be 7.902 gm/cm³ at 22°C.

The results also show that the specimen volume change by void formation (swelling) determined from the TEM data closely approximates that determined by immersion density change. Figures 6a and 6b show the mean void diameter and void number density data as functions of the irradiation temperature. The swelling calculated from the respective void diameters and number densities is shown in Fig. 6c. For comparison, the swelling determined by the immersion density method is shown in Fig. 1c as a function of specimen location in EBR-II. From Table 1 and Figs. 1c and 6a-c, it is seen that the maximum swelling occurred concurrently with the maximum mean void diameter, slightly above the maximum fluence location, and slightly below the maximum observed void number density. The peak shown in Fig. 6a indicates the substantial effect of neutron fluence on the void diameter. In all cases, the present void parameters are consistent with previously published results for neutron-irradiated Type 304 stainless steel [1-7,14].

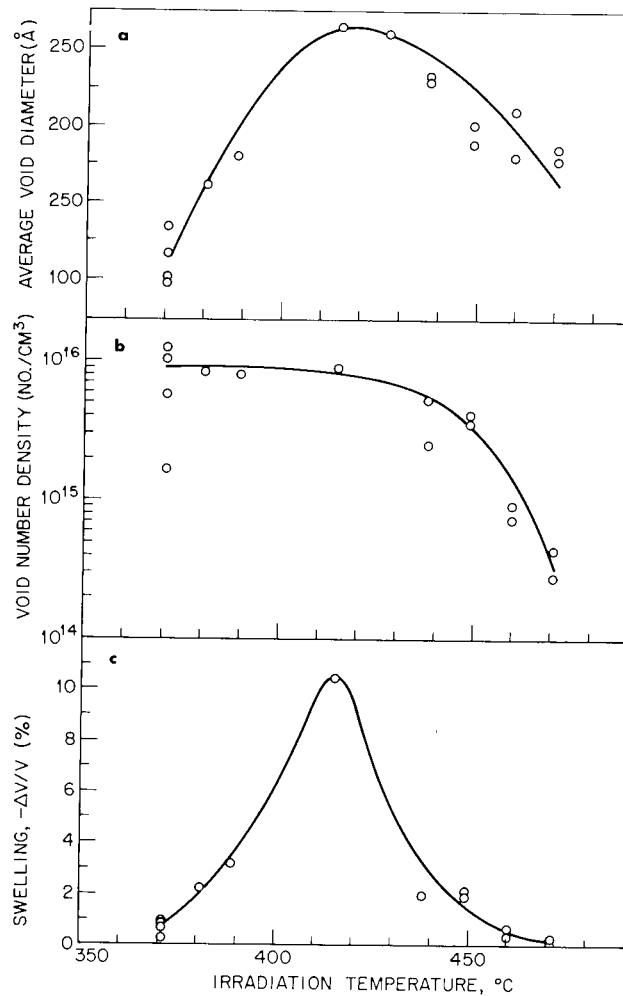


Fig. 6 — Mean void diameter (a), void number density (b), and swelling (c) as a function of irradiation temperature for annealed Type 304 stainless steel (EBR-II control rod thimble 5D3)

The dislocation densities determined from the TEM results are given in Table 1, and Figs. 7a-7f illustrate typical dislocation and loop structures observed in all specimens. At the lower irradiation temperatures and fluences, as shown in Fig. 7a, defect clusters, small dislocation loops, and dislocation segments were predominant throughout the material. Near the peak fluence and at higher irradiation temperatures, a dislocation network connected all voids as seen in Figs. 7b-7d. The development of Frank-faulted loops was observed for those specimens irradiated at the highest temperatures but to lower fluences, Figs. 7e and 7f.

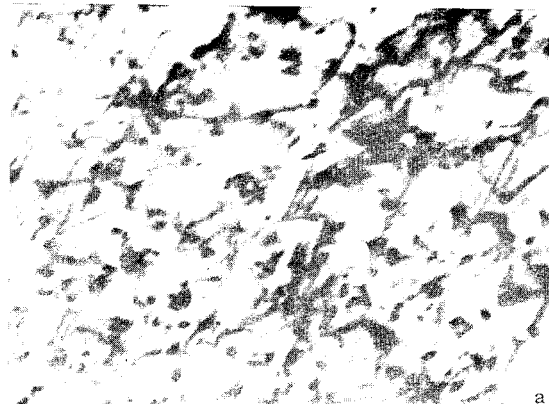
No attempt was made to obtain complete quantitative data for the dislocation loops observed during the TEM examination. However, qualitative observations indicated that the number density of small voids was considerably higher for those specimens irradiated at temperatures between 370 and 380°C, Figs. 7a and 7b, for example, than for those specimens irradiated at temperatures between 450 and 480°C. Within the higher irradiation temperature range, the Frank-faulted loop concentrations were found to decrease from $2 \times 10^{15} / \text{cm}^3$ to $3 \times 10^{14} / \text{cm}^3$ with decreasing neutron fluence.

The immersion density results presented in Fig. 1c are compared in Fig. 8 with the density decrease calculated according to the empirical expression developed for use with the LIFE II fuel element performance code [30]. The comparison in Fig. 8 shows that the calculated density decrease is greater than the experimental values except for those specimens irradiated at the lower temperatures in locations below the core midplane. At the position of maximum swelling, the calculated density decrease is seen to overestimate the observed decrease by nearly 50%. This suggests that the empirical expression may require revision to more accurately represent the swelling actually observed in Type 304 stainless steel during long-term breeder reactor exposure.

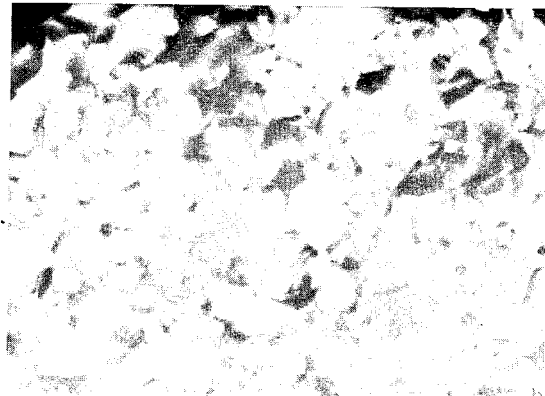
The microhardness measurement results given in Table 1 are shown in Fig. 9 as a function of specimen location in EBR-II. The test temperatures indicated on both Figs. 9a and 9b refer to the temperatures at which postirradiation fatigue tests were conducted. For all specimens, the microhardness increments ΔH shown in Figs. 9a and 9b by the individual data points and their heavy connecting curve were determined according to the expression

$$\Delta H = H_{\text{irr}} - H_{\text{unirr}}, \quad (2)$$

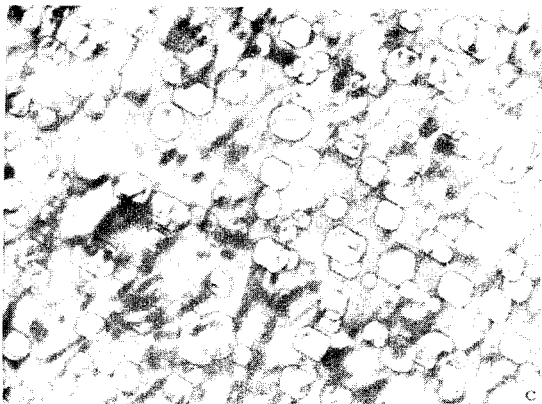
where H_{irr} is the ambient temperature postirradiation microhardness of the irradiated material and H_{unirr} is the ambient temperature microhardness of the unirradiated annealed Type 304 stainless steel thimble material. This measurement produces a direct indication of the radiation-induced defect strengthening as well as effects of any subsequent thermal treatment on the strengthening. The curves in Figs. 9a and 9b identified as voids only and voids and dislocations represent the microhardness contribution of the voids as well as both voids and dislocations as computed from the TEM results. The separate contributions of the voids and the dislocations to the microhardness increment were calculated according to the expressions



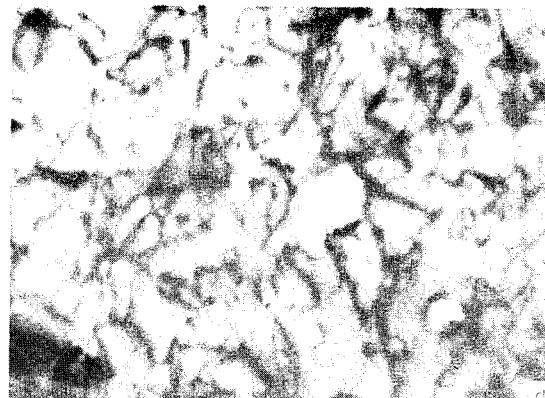
$T_{\text{irrad}} = 371^{\circ}\text{C}$, $\phi t = 1.3 \times 10^{22} \text{ n/cm}^2$



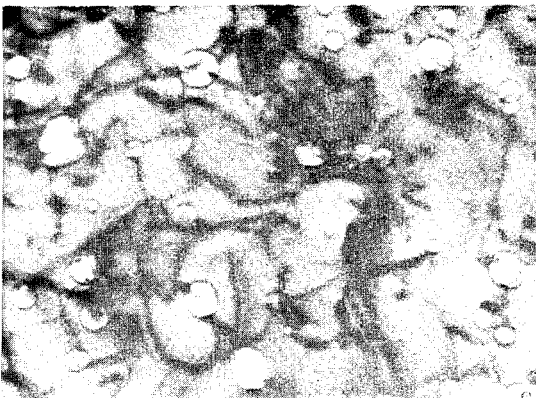
$T_{\text{irrad}} = 382^{\circ}\text{C}$, $\phi t = 1.3 \times 10^{22} \text{ n/cm}^2$



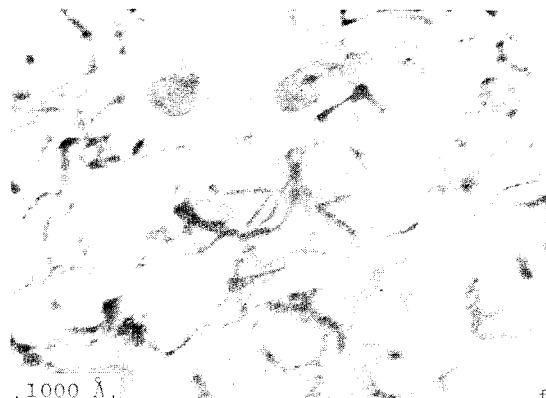
$T_{\text{irrad}} = 438^{\circ}\text{C}$, $\phi t = 1.0 \times 10^{22} \text{ n/cm}^2$



$T_{\text{irrad}} = 449^{\circ}\text{C}$, $\phi t = 7.0 \times 10^{21} \text{ n/cm}^2$



$T_{\text{irrad}} = 460^{\circ}\text{C}$, $\phi t = 1.4 \times 10^{22} \text{ n/cm}^2$



$T_{\text{irrad}} = 471^{\circ}\text{C}$, $\phi t = 9.0 \times 10^{21} \text{ n/cm}^2$

Fig. 7 — Transmission electron micrographs of dislocations and loops in neutron-irradiated Type 304 stainless steel (EBR-II control rod thimble 5D3)

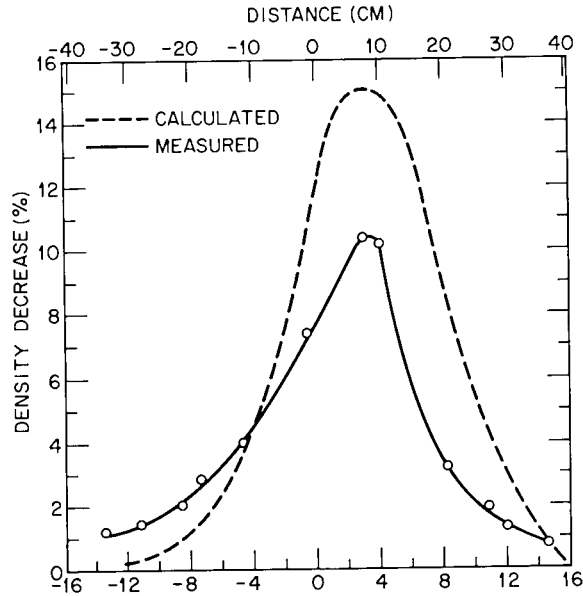


Fig. 8 — Measured and calculated immersion density decrease as a function of specimen position for neutron-irradiated Type 304 stainless steel (EBR-II control rod thimble 5D3)

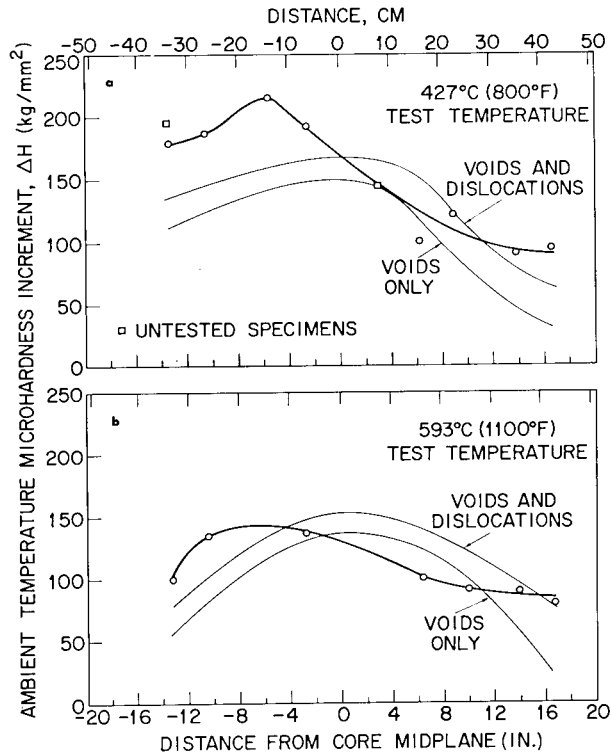


Fig. 9 — Measured and calculated microhardness increment (a and b) as a function of specimen position for neutron-irradiated Type 304 stainless steel (EBR-II control rod thimble 5D3)

$$\Delta H_{\text{voids}} = 6\alpha\mu b (N_v d_v)^{1/2} \quad (3)$$

$$\Delta H_{\text{disl}} = 6\alpha\mu b (\rho_d)^{1/2} \quad (4)$$

where

μ is the shear modulus

b is the Burgers vector

N_v is the void number density

d_v is the mean void diameter

ρ_d is the dislocation density (dislocations/cm²)

α is a dislocation-defect interaction parameter determining the barrier strength and assumed to be a constant.

For the present calculations, the values $\alpha = 1$ for voids and $\alpha = 1/2$ for dislocations were used since previous work has shown that these values produce reasonable agreement between the calculated and experimental microhardness increments for irradiated materials [31]. The shear moduli values used in the calculations were determined from acoustical measurements of the shear modulus as a function of immersion density decrease for Type 304 stainless steel thimble material which received EBR-II irradiation temperature and fluence exposures very similar to that received by the thimble material used in the present study [32]. The combined contribution of both the voids and the dislocations to the microhardness ΔH_{total} was computed according to the expression

$$\Delta H_{\text{total}} = \left[(\Delta H_{\text{voids}})^2 + (\Delta H_{\text{disloc}})^2 \right]^{1/2}. \quad (5)$$

Examination of Figs. 9a and 9b shows that the measured microhardness increments directly reflect the irradiation temperature and fluence gradients experienced by the material. Comparison of the figures, however, also indicates the substantial effect of prior exposure at the fatigue test temperatures. For specimens from locations below the EBR-II core midplane, the difference between the microhardness increments measured for specimens previously fatigue tested at 427 and 593°C is seen to be considerable, whereas above the core midplane this difference becomes almost negligible. Inspection of the irradiation temperature profile shown in Fig. 1a suggests that the basic reason for the microhardness increment differences is primarily the effect of test temperature on the radiation-induced defect structure. For specimens exposed to the 427°C fatigue test

temperature, this temperature was higher than the irradiation temperature for specimens located lower than approximately 12.5 cm above the reactor core midplane. This indicates that the test temperature—irradiation temperature differential has promoted the partial recovery of the radiation-induced defects in these specimens to produce the decrease in microhardness increment measured for specimen locations near the lower end of the thimble material. Microhardness increment measurements on thimble material not exposed to 427°C fatigue test temperature substantiate this effect as shown by those points identified as being from untested specimens in Fig. 9a. The importance of this apparent recovery is further illustrated by the microhardness increments measured for those specimens previously exposed to 593°C fatigue test temperature, Fig. 9b, where a similar but more pronounced microhardness increment reduction has occurred for specimens whose locations were identical to those in Fig. 9a. Thus, the measurements strongly suggest that these recovery effects coupled with the irradiation temperature and fluence gradients have produced the maxima in the measured microhardness increment curves shown in Figs. 9a and 9b rather than the expected continuous increment increase toward the lower end of the control rod thimble.

The curves shown in Figs. 9a and 9b for the microhardness increments calculated using Eqs. (3)-(5) are seen to reflect generally the overall trends followed by the experimentally measured values, including the differences due to specimen exposure at the fatigue test temperatures. In both figures, the primary microstructural component contributing to the calculated microhardness increments are the voids. As expected, the microhardness increments calculated for the combined contributions of both voids and dislocations is higher for all specimens than those due to the voids only. However, a direct comparison of the calculated and measured values reveals important differences that are indicative of the microstructure.

For specimen locations below the reactor core midplane in both Figs. 9a and 9b, the calculated microhardness increments are considerably below the experimental values. Because the measured microhardness increments include the contribution of all components of the microstructure while the calculated values pertain only to the increments from specific components, the difference between the calculated and experimental values for specimens below the core midplane results from microstructural components not included in the calculation. Previously in this report it was indicated that small dislocation loops and defect clusters were prominent microstructural features of those thimble specimens irradiated at the lower temperatures. This strongly suggests that the small dislocation loops and defect clusters account for the difference between the calculated and measured microhardness increments for these specimen locations. However, at specimen locations near or slightly above the core midplane, the calculated values exceed or equal the measured values. This effect is more pronounced in Fig. 9b than in 9a and indicates that the calculations overestimate the microhardness increment contribution of the voids and dislocations for specimens irradiated near the core midplane. Because the voids are the primary microstructural feature that contributes to the calculated microhardness increment, it is reasonable to expect that the variation of the mean void diameter and void number density with irradiation temperature and neutron fluence could account for the overestimate. Figure 6a suggests that the mean void diameter, rather than the void number density, Fig. 6b, is mainly responsible because this void parameter exhibits the largest variation with the irradiation conditions. The possible

contribution of the specimen exposure to the fatigue test temperatures on the calculated microhardness increments, and hence on the difference between the calculated and measured values, is considered to be minimal for those specimens located near and slightly above the core midplane because the void parameters show little variation with test temperature in Table 1. Thus, the void parameters, as influenced by the irradiation temperature and fluence conditions, coupled with possible measurement errors, provide the primary contribution to the calculated and measured microhardness increment differences near the core midplane.

The results obtained in this study have shown that the radiation-induced voids are the major microstructural feature influencing the microhardness of the Type 304 stainless steel. Because it is known that the microhardness of any material directly reflects the flow properties of the material, [33,34], it is concluded that the voids will be the primary component affecting the plastic flow properties of the thimble material. Minor contributions to the plastic flow properties will be provided by the dislocations, loops, and defect clusters. This suggests that the fatigue behavior of the thimble material reported previously [27] may be understood on the basis of the radiation-induced defect structure. However, additional experiments will be necessary to define carefully and completely the microstructure vs flow properties vs fatigue relationships for neutron-irradiated stainless steels similar to that employed in this study.

SUMMARY AND CONCLUSIONS

The microstructure, swelling, and microhardness of annealed Type 304 stainless steel were evaluated for EBR-II control rod thimble material that received fluences near 1.6×10^{23} n/cm² > 0.1 MeV at irradiation temperatures from 370 to 470°C (698 to 878°F). All results show the strong influence of the irradiation temperature and fluence gradients experienced by the material. The following conclusions were drawn from the results of this investigation:

1. The maximum swelling determined by immersion density measurements and independently confirmed by transmission electron microscopy was 10.4% at an irradiation temperature of 415°C.
2. Swelling calculated according to the LIFE II fuel element performance code exceeded that determined for the thimble material from immersion density measurements by nearly 50% at the location of maximum swelling.
3. Ambient temperature microhardness measurements show general agreement with microhardness values calculated from the electron microscopy data.
4. Radiation-induced voids are the primary microstructural component contributing to the measured microhardness.
5. Based on the relationship between microhardness and flow properties, it is concluded that voids are the major microstructural component that will influence the plastic flow properties of the thimble material.

ACKNOWLEDGMENTS

This work was supported by the U.S. Atomic Energy Commission and the Office of Naval Research.

REFERENCES

1. E.E. Bloom, "Nucleation and Growth of Voids in Stainless Steels During Fast-Neutron Irradiation," in *Radiation-Induced Voids in Metals* (J.E. Corbett and L.C. Ianniello, editors), USAEC Symposium Series 26, U.S. Atomic Energy Commission, Washington, D.C., 1972, p. 1.
2. E.E. Bloom, J.O. Stiegler, and C.J. McHargue, "Radiation Damage in Annealed Type 304 Stainless Steel," *Radiation Effects* 14, 231 (1972).
3. S.D. Harkness and Che-Yu Li, "A Study of Void Formation in Fast Neutron Irradiated Metals," *Met. Trans.* 2, 1457 (1971).
4. W.K. Appleby, D.W. Sandusky, and U.E. Wolff, "Fluence and Temperature Dependence of Void Formation in Highly Irradiated Stainless Steels," in *Radiation-Induced Voids in Metals* (J.W. Corbett and L.C. Ianniello, editors), USAEC Symposium Series 26, U.S. Atomic Energy Commission, Washington, D.C., 1972, p. 156.
5. H.R. Brager, J.L. Straalsund, J.J. Holmes, and J.F. Bates, "Irradiation-Produced Defects in Austenitic Stainless Steel," *Met. Trans.* 2, 1893 (1971).
6. R.L. Fish, J.L. Straalsund, C.W. Hunter, and J.J. Holmes, "Swelling and Tensile Property Evaluations of High-Fluence EBR-II Thimbles," in *Effects of Radiation on Substructure and Mechanical Properties of Metals and Alloys*, ASTM STP 529, 1973, p. 149.
7. R. Carlander, S.D. Harkness, and F.L. Yaggee, "Fast-Neutron Effects on Type 304 Stainless Steel," *Nucl. Appl. Technol.* 7, 67 (1969).
8. D.W. Sandusky, C.N. Spalaris, and U.E. Wolff, "Irradiation Temperature Dependence of Void Formation in Type-304 Stainless Steel," *J. Nucl. Mater.* 42, 133 (1972).
9. J.O. Stiegler, and E.E. Bloom, "The Effect of Thermo-Mechanical Treatments on Void Formation in Irradiated Stainless Steel," *J. Nucl. Mater.* 41, 341 (1971).
10. H.R. Brager and J.L. Straalsund, "Microstructure of Neutron-Irradiated Solution-Treated Type 316 Stainless Steel," *Trans. Amer. Nucl. Soc.* 15, 725 (1972).
11. H.R. Brager and J.L. Straalsund, "Irradiation Temperature Dependence of Void Formation in Cold-Worked Type 316 Stainless Steel," *J. Nucl. Mater.* 46, 103 (1973).

12. H.R. Brager and J.L. Straalsund, "Defect Development in Neutron Irradiated Type 316 Stainless Steel," *J. Nucl. Mater.* **46**, 134 (1973).
13. J.J. Holmes, A.J. Lovell, and R.L. Fish, Ductility of Irradiated Type 316 Stainless Steel," in *Effects of Radiation on Substructure and Mechanical Properties of Metals and Alloys*, ASTM STP 529, 1973, p. 383.
14. J.J. Holmes, R.E. Robbins, J.L. Brimhall, and B. Mastel, "Elevated Temperature Irradiation Hardening in Austenitic Stainless Steel," *Acta. Met.* **16**, 955 (1968).
15. M. Weisz, J. Malkin, J. Efler, and J.P. Andre, "High-Temperature Embrittlement of AISI Type 316 Austenitic Stainless Steels after Irradiation," in *Irradiation Effects in Structural Alloys for Thermal and Fast Reactors*, ASTM STP 457, 1969, p. 352.
16. E.E. Bloom and J.R. Weir, Jr., "Effect of Neutron Irradiation on the Ductility of Austenitic Stainless Steel," *Nucl. Technol.* **16**, 45 (1972).
17. E.E. Bloom and J.O. Stiegler, "Effect of Irradiation on the Microstructure and Creep-Rupture Properties of Type 316 Stainless Steel," in *Effects of Radiation on Substructure and Mechanical Properties of Metals and Alloys*, ASTM STP 529, 1973, p. 360.
18. A.J. Lovell and R.W. Barker, "Uniaxial and Biaxial Creep Rupture of Type 316 Stainless Steel After Fast Reactor Irradiation," in *Irradiation Effects on Structural Alloys for Nuclear Reactor Applications*, ASTM STP 484, 1970, p. 468.
19. A.J. Lovell, "Postirradiation Creep of Annealed Type 316 Stainless Steel," *Nucl. Technol.* **16**, 323 (1972).
20. E.E. Bloom and J.O. Stiegler, "Effect of Fast Neutron Irradiation on the Creep Rupture Properties of Type 304 Stainless Steel at 600 C," in *Irradiation Effects on Structural Alloys for Nuclear Reactor Applications*, ASTM STP 484, 1970, p. 451.
21. J.M. Beeston and C.R. Brinkman, "Axial Fatigue of Irradiated Stainless Steels Tested at Elevated Temperatures," in *Irradiation Effects on Structural Alloys for Nuclear Reactor Applications*, ASTM STP 484, 1970, p. 419.
22. C.R. Brinkman, G.E. Korth, and J.M. Beeston, "Influence of Irradiation on the Creep/Fatigue Behavior of Several Austenitic Stainless Steels and Incoloy 800 at 700 C," in *Effects of Radiation on Substructure and Mechanical Properties of Metals and Alloys*, ASTM STP 529, 1973, p. 473.
23. C.R. Brinkman, G.E. Korth, and R.R. Hobbins, "Estimates of Creep-Fatigue Interaction in Irradiated and Unirradiated Austenitic Stainless Steels," *Nucl. Technol.* **16**, 297 (1972).

24. C.R. Brinkman, G.E. Korth, and J.M. Beeston, "Comparison of the Fatigue and Creep-Fatigue Properties of Unirradiated and Irradiated Type 304 and 316 Stainless Steel at 593 C (1100 F)," ANCR-1078, Aerojet Nuclear Company, Idaho Falls, Idaho, Aug. 1972.
25. P. Shahinian, H.E. Watson, and H.H. Smith, "Effect of Neutron Irradiation on Fatigue Crack Propagation in Types 304 and 316 Stainless Steel at High Temperatures," in *Effects of Radiation on Substructure and Mechanical Properties of Metals and Alloys*, ASTM STP 529, 1973, p. 493.
26. L.A. James and R.L. Knecht, "Fatigue-Crack Propagation in Fast-Neutron-Irradiated Types-304 and -316 Stainless Steels," *Nucl. Technol.* **19**, 148 (1973).
27. D.J. Michel and H.H. Smith, "Fatigue Behavior and Microstructure of Neutron Irradiated Thin Section Type 304 Stainless Steel at Elevated Temperatures," in *Effects of Radiation on Structural Materials*, ASTM STP (to be published).
28. R.D. Schoone and E.A. Fischione, "Automatic Unit for Thinning Transmission Electron Microscopy Specimens of Metals," *Rev. Sci. Instr.* **37**, 1351 (1966).
29. R.J. Ratcliffe, "The Measurement of Small Density Changes in Solids," *Brit. J. Appl. Phys.* **16**, 1193 (1965).
30. R.D. Leggett, E.O. Ballard, F.E. Bard, J.W. Weber, L.A. Pember, and R.J. Jackson, "Correlation of Predictions and Observations in Mixed-Oxide Fuel," *Trans. Amer. Nucl. Soc.* **13**, 574 (1970).
31. J. Moteff, D.J. Michel, and V. Sikka, "The Influence of Irradiation Temperature on the Hardening Behavior of the Refractory B.C.C. Metals and Alloys," in *Defects and Defect Clusters in B.C.C. Metals and Their Alloys*, (R.J. Arsenault, editor), *Nuclear Metallurgy*, **18**, American Institute of Mining, Metallurgical and Petroleum Engineers, New York, 1973, p. 198.
32. R.L. Trantow, "Ultrasonic Measurement of Elastic Properties in Irradiated 304 Stainless Steel," HEDL-TME-73-92, Hanford Engineering Development Laboratory, Westinghouse Hanford Company, Richland, Wash., Dec. 1973.
33. J.R. Cahoon, "An Improved Equation Relating Hardness to Ultimate Strength," *Met. Trans.* **3**, 3040 (1972).
34. J. Moteff and P.R. Sieber, "A Correlation Between the Hot-Hardness and the Hot-Tensile Properties of AISI 304 Stainless Steel," *Met. Trans.* **5**, 315 (1974).